Mechanics of Advanced Materials and Structures
Publication details, including instructions for authors and subscription information:
http://www.tandfonline.com/loi/umcm20

Analysis of FGM Beams by Means of Classical and Advanced Theories

G. Giunta [a], S. Belouettar [b] & E. Carrera [c]
[a] Centre de Recherche Public Henri Tudor, Luxembourg and Politecnico di Torino, Turin, Italy
[b] Centre de Recherche Public Henri Tudor, Luxembourg-Kirchberg, Luxembourg
[c] Politecnico di Torino, Turin, Italy
Published online: 25 Nov 2010.

To cite this article: G. Giunta, S. Belouettar & E. Carrera (2010) Analysis of FGM Beams by Means of Classical and Advanced Theories, Mechanics of Advanced Materials and Structures, 17:8, 622-635, DOI: 10.1080/15376494.2010.518930

To link to this article: http://dx.doi.org/10.1080/15376494.2010.518930

Mechanics of Advanced Materials and Structures, 17:622–635, 2010

ISSN: 1537-6494 print / 1537-6532 online
DOI: 10.1080/15376494.2010.518930

Taylor & Francis
Taylor & Francis Group

Analysis of FGM Beams by Means of Classical and Advanced Theories

G. Giunta,[1] S. Belouettar,[2] and E. Carrera[3]

[1]*Centre de Recherche Public Henri Tudor, Luxembourg and Politecnico di Torino, Turin, Italy*
[2]*Centre de Recherche Public Henri Tudor, Luxembourg-Kirchberg, Luxembourg*
[3]*Politecnico di Torino, Turin, Italy*

This paper proposes several axiomatic refined theories for the linear static analysis of beams made of materials whose properties are graded along one or two directions. Via a unified formulation, a generic N-order approximation is assumed for the displacement unknown variables over the beam cross-section. The governing differential equations and the boundary conditions are derived in terms of a fundamental nucleo that does not depend upon the approximation order. A Navier type, closed form solution is adopted. Classical beam theories, such as Euler-Bernoulli's and Timoshenko's, are obtained as particular cases. Beams that undergo bending and torsional loadings are investigated. Several values of the span-to-height ratio are considered. Slender as well as deep beams are, therefore, investigated. Comparisons with elasticity solutions and three-dimensional finite element models are given. The numerical investigation shows that the proposed unified formulation yields the complete three-dimensional displacement and stress fields as long as the appropriate approximation order is considered. The accuracy of the solution depends upon the geometrical parameters of the beam and the loading conditions.

Keywords axiomatic refined beam theories, unified formulation, functionally graded materials, Navier-type solution

1. INTRODUCTION

Functionally Graded Materials (FGMs) are composed of two or more materials whose volume fraction changes gradually along desired spatial directions resulting in a smooth and continuous change in the effective properties. The combination of different materials with specific physical properties allows a tailored material design that broadens the structural design space by implementing a multi-functional response with a minimal weight increase. The concept of FGM was developed by Japanese material scientists in 1984 for super heat resistant materials to be used in space-planes or nuclear fusion reactors. The first feasibility study on "The basic technology for the development of functionally gradient materials for relaxation of thermal stresses" was performed in 1986 (see Koizumi [1]). At the end of the study, a square shell of SiC-C FGM for the base of the fuselage of space-planes was fabricated. The gradual and smooth change in the material profile and in the effective physical properties achievable by FGMs makes them distinguishable from the conventional composites since the mismatch that is often encountered in laminated composites and is known to promote delamination-related problems can be eliminated (see Reddy [2]); in-plane and transverse through the-thickness stresses can be reduced (see Aboudi et al. [3]); the residual stress distribution can be improved (see Shabana and Noda [4]); the fracture toughness canbe enhanced (see Erdogan [5]); the stress intensity factors can be reduced (see Xiao et al. [6]); and the fatigue life can be increased (see Jian et al. [7]). FGMs are, therefore, preferable in many engineering applications such as energy conversion (see Koizumi [1]), dental and orthopaedic implants (see Pompe et al. [8]), sensors and thermo-generators (see Müller et al. [9]), and wear resistant coatings (see Schulz et al. [10]). As far as structural applications are concerned, the study of beam structures made of FGMs represents an important topic of research since many primary and secondary structural elements, such as aircraft wings, helicopter rotor blades or robot arms can be idealised as beams. A general account of FGMs (design, fabrication and applications) can be found in Suresh and Mortensen [11], Miyamoto et al. [12], and Watanabe et al. [13]. As far as the micro-mechanics of FGMs is concerned, a review of classical approaches such as self-consistent schemes (see Hill [14]), differential schemes, Mori and Tanaka's method [15], and concentric cylinder models can be found in Aboucdi [16], Nemat-Nasser and Hori [17] and Zuiker and Dvorak [18]. To the best of the authors' knowledge, one of the first micro-mechanical approaches developed especially for FGMs was proposed by Wakashima and Tsukamoto [19]. Pindera et al. [20] demonstrated that classical methods cannot be profitably applied to FGMs since they decouple the local response from the global one. Aboudi et al. [21, 22, 3] introduced a higher order theory for FGMs based on a volumetric averaging approach that explicitly

Received 29 July 2009; accepted 11 September 2009.
Address correspondence to Gaeatano Giunta, Ph.D., Department of Advanced Materials and Structures, Centre de Recherche Public Henri Tudor, 29, av. John F. Kennedy, L-1855, Luxembourg-Kirchberg, Luxembourg. E-mail: gaetano.giunta@tudor.lu

couples micro- and macro-scale with spatially varying microstructures in one, two and three orthogonal directions. Regarding the modelling of FGMs-based structures, Chakraborty et al. [23] developed a finite element based on Timoshenko's beam theory (TB) (see Timoshenko [24, 25] and Timoshenko and Goodier [26]) in which the shape functions have been derived from the general exact solution of the static governing equations. Exponential and polynomial gradation of mechanical and thermal properties along the through-the-thickness direction were accounted for. Static, free vibration and wave propagation analyses were accounted for. Li [27] proposed a unified approach to the formulation of Timoshenko's and Euler-Bernoulli's (EB) beam models. The same analyses as in [23] were performed. Young's modulus varied along the transverse coordinate according to a power-law function. Kadoli et al. [28] proposed a finite element based on a third-order approximation of the axial displacement and constant transverse displacement for the static analysis of beams made of metal-ceramic FGMs. Components' volume fraction was supposed to vary according to a power-law function. A discrete layer approach was adopted to account for material gradation. Kapuria et al. [29] proposed a finite element based on a third-order, zig-zag theory for the static and free vibration analysis of Al/SiC and Ni/Al_2O_2 layered functionally graded beams. The hypothesis of plane stress was adopted. The normal stress along the thickness direction was neglected. The effective Young's modulus was computed via the modified rule of mixture that was proposed by Tomota et al. [30] for cemented carbides. Poisson's ratio and material density were computed by means of linear rule of mixture. A polynomial variation of the volume fractions of the constituents along the thickness was adopted. The theoretical model was validated toward experimental results. Sallai et al. [31] investigated beams made of sigmoid FGMs (S-FGMs) via classical and higher order models accounting for linear, parabolic and exponential shear deformation. The transverse displacement was assumed to be constant versus the thickness coordinate. In S-FGM, the volume fraction of the constituents varies according to two power-law functions in order to avoid stress concentration typical of a single power-law function and steep gradation of the material properties (see Chung and Chi [32]). As far as elasticity solutions are concerned, Sankar [33] solved the plane elasticity equations exactly. An EB type theory was also derived. The shear stress component was obtained via integration of the indefinite equilibrium equations. Simply supported, FGM beams subjected to sinusoidal loadings were investigated. Young's modulus was supposed to vary exponentially along the thickness direction, while Poisson's ratio was constant. Zhu and Sankar [34] adopted a combined Fourier series-Galerkin method for the analysis of simply supported FGM-based beams for which the Young's modulus was a third-order polynomial function of the through-the-thickness coordinate. The Poisson ratio was constant. The basis functions were the elements of the classical polynomial base up to the third-order versus the thickness direction. Under the hypothesis of plane stress, Ding et al. [35] generalised Silverman's method (see Silverman [36]) in order to obtain a stress function for anisotropic functionally graded beams in a general manner. The governing equations were derived independently from the variation of the elastic compliance parameters along the beam thickness. Cantilever, simply supported and fixed-fixed beams were studied. Body forces were also accounted for. An exponential function was assumed for the material compliance coefficient S_{11} while the others were considered constant. The present paper proposes a systemic manner of formulating axiomatically refined beam models. Via a concise notation for the kinematic field, the governing differential equations and the corresponding boundary conditions are reduced to a "fundamental nucleo" in terms of the displacement components. The fundamental nucleo does not depend upon the approximation order. This is, therefore, assumed as free parameter of the formulation. This formulation is named Carrera's Unified Formulation and it was previously applied to the modelling of anisotropic plate and shell structures (see Carrera [37]). In particular, Carrera et al. [38] and Brischetto and Carrera [39] proposed several hierarchical models on the basis of the principle of virtual displacement and Reissner's mixed variational theorem (see Reissner [40]) for the static analysis of FGMs-based plates. Brischetto et al. [41] applied displacement-based models to the fully thermo-mechanical analysis of plates made of monel-ceramic-zirconia FGM. Displacement-based theories that account for non-classical effects, such as transverse shear and in- and out-of-plane warping of the cross-section, can be formulated. It is worth mentioning that no special warping functions need to be assumed. Classical models, such as EB and TB, can be retrieved as particular cases. Navier's closed form solution is adopted to solve the governing differential equation. Slender and deep beams are investigated. Isotropic FGMs are accounted for. Young's modulus is considered to vary exponentially along two perpendicular directions on the cross-section. Poisson's ration is constant, since its effect on the deformation is much less than that of Young's modulus (see Delale and Erdogan [42]). The proposed models are validated towards elasticity exact solutions or three-dimensional finite element models (FEM) that have been appositely developed.

2. PRELIMINARIES

A beam is a structure whose axial extension, l, is predominant compared to any other dimension orthogonal to it. The cross-section, Ω, is identified by intersecting the beam with planes that are orthogonal to its axis. Cross-sections that are obtainable by the union of N_{Ω^k} rectangular sub-domains:

$$\Omega = \bigcup_{k=1}^{N_{\Omega^k}} \Omega^k \tag{1}$$

with:

$$\Omega^k = \left\{(y, z) : y_1^k \leq y \leq y_2^k; \quad z_1^k \leq z \leq z_2^k\right\} \tag{2}$$

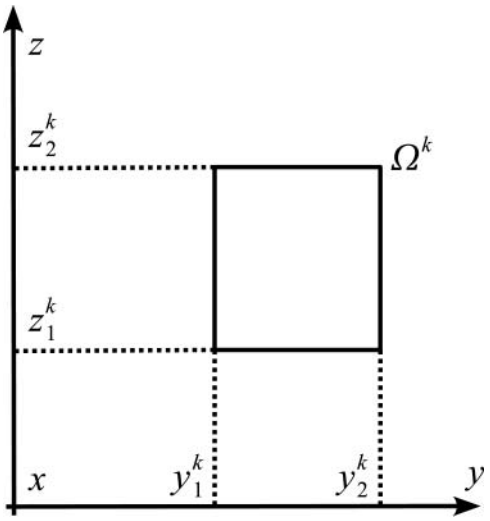

FIG. 1. Generic rectangular k sub-domain.

are considered, see Fig 1. Terms $\{(y_i^k, z_j^k) : i, j = 1, 2\}$ are the coordinates of the corner points of k sub-domain. Through the paper, superscript "k" represents the cross-section sub-domain index, while, as subscript, it stands for summation over the range $(1, N_{\Omega^k})$. A Cartesian reference system is adopted: y- and z-axis are two orthogonal directions laying on the cross-section. The x coordinate is coincident to the axis of the beam. It is bounded such that $0 \leq x \leq l$. The cross-section is considered constant along x. The displacement field is:

$$\mathbf{u}^T(x, y, z) = \{u_x(x, y, z)\ u_y(x, y, z)\ u_z(x, y, z)\} \tag{3}$$

in which u_x, u_y, and u_z are the displacement components along x-, y- and z-axes. Superscript "T" represents the transposition operator. The stress, σ, and strain, ε, vectors are grouped into vectors σ_n, ε_n that lay on the cross-section:

$$\begin{aligned} \sigma_n^T &= \{\, \sigma_{xx}\ \sigma_{xy}\ \sigma_{xz}\,\} \\ \varepsilon_n^T &= \{\, \varepsilon_{xx}\ \varepsilon_{xy}\ \varepsilon_{xz}\,\} \end{aligned} \tag{4}$$

and σ_p, ε_p laying on planes orthogonal to Ω:

$$\begin{aligned} \sigma_p^T &= \{\, \sigma_{yy}\ \sigma_{zz}\ \sigma_{yz}\} \\ \varepsilon_p^T &= \{\, \varepsilon_{yy}\ \varepsilon_{zz}\ \varepsilon_{yz}\} \end{aligned} \tag{5}$$

In the case of small displacements with respect to a characteristic dimension of Ω, linear relations between strain and displacement components hold:

$$\begin{aligned} \boldsymbol{\varepsilon}_n^T &= \{\, u_{x,x}\ u_{x,y} + u_{y,x}\ u_{x,z} + u_{z,x}\,\} \\ \boldsymbol{\varepsilon}_p^T &= \{\, u_{y,y}\ u_{z,z}\ u_{y,z} + u_{z,y}\,\} \end{aligned} \tag{6}$$

Subscripts "x", "y" and "z", when preceded by comma, represent derivation versus the corresponding spatial coordinates. A compact vectorial notation can be adopted for Eq. (6):

$$\begin{aligned} \varepsilon_n &= \mathbf{D}_{np}\mathbf{u} + \mathbf{D}_{nx}\mathbf{u} \\ \varepsilon_p &= \mathbf{D}_p\mathbf{u} \end{aligned} \tag{7}$$

where $\mathbf{D}_{np}$, $\mathbf{D}_{nx}$, and $\mathbf{D}_p$ are the following differential matrix operators:

$$\mathbf{D}_{np} = \begin{bmatrix} 0 & 0 & 0 \\ \dfrac{\partial}{\partial y} & 0 & 0 \\ \dfrac{\partial}{\partial z} & 0 & 0 \end{bmatrix} \quad \mathbf{D}_{nx} = \mathbf{I}\frac{\partial}{\partial x} \quad \mathbf{D}_p = \begin{bmatrix} 0 & \dfrac{\partial}{\partial y} & 0 \\ 0 & 0 & \dfrac{\partial}{\partial z} \\ 0 & \dfrac{\partial}{\partial z} & \dfrac{\partial}{\partial y} \end{bmatrix} \tag{8}$$

where $\mathbf{I}$ is the unit matrix. Under the hypothesis of isotropic linear elastic FGMs, the generalised Hooke law holds. Its compact vectorial form is:

$$\boldsymbol{\sigma} = \mathbf{C}(y, z)\varepsilon \tag{9}$$

in which $\mathbf{C}$ is the material stiffness matrix accounting for properties gradation along the directions y and z. According to Eqs. (4) and (5), Eq. (9) reads:

$$\begin{aligned} \boldsymbol{\sigma}_p &= \mathbf{C}_{pp}(y, z)\varepsilon_p + \mathbf{C}_{pn}(y, z)\varepsilon_n \\ \boldsymbol{\sigma}_n &= \mathbf{C}_{np}(y, z)\varepsilon_p + \mathbf{C}_{nn}(y, z)\varepsilon_n \end{aligned} \tag{10}$$

As far as the material properties are concerned, Young's modulus, E, is supposed to vary with respect to y and z coordinates according to the following exponential law:

$$E(y, z) = E_0 e^{(\alpha_1 y + \beta_1)} e^{(\alpha_2 z + \beta_2)} \tag{11}$$

Figure 2 presents the variation of E/E_0 versus y and z over a rectangular cross-section. Poisson's ratio, ν is considered

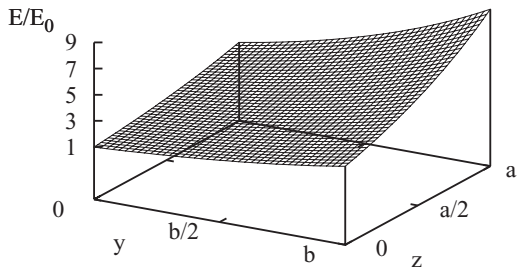

FIG. 2. E/E_0 variation over beam cross-section; α_1 and α_2 in Eq. (11) such that $E(b, 0)/E_0 = E(0, a)/E_0 = 3$ and $\beta_1 = \beta_2 = 0$.

TABLE 1
Mac Laurin's polynomials via Pascal's triangle

N	N_u	F_τ
0	1	$F_1 = 1$
1	3	$F_2 = yF_3 = z$
2	6	$F_4 = y^2\ F_5 = yz\ F_6 = z^2$
3	10	$F_7 = y^3\ F_8 = y^2z\ F_9 = yz^2\ F_{10} = z^3$
...	...	...
N	$\frac{(N+1)(N+2)}{2}$	$F_{\frac{(N^2+N+2)}{2}} = y^N\ F_{\frac{(N^2+N+4)}{2}} = y^{N-1}z \cdots F_{\frac{N(N+3)}{2}} = yz^{N-1}\ F_{\frac{(N+1)(N+2)}{2}} = z^N$

constant. Matrixes $\mathbf{C}_{pp}$, $\mathbf{C}_{pn}$, $\mathbf{C}_{np}$ and $\mathbf{C}_{nn}$ in Eqs. (10) are:

$$\mathbf{C}_{pp} = \begin{bmatrix} C_{22} & C_{23} & 0 \\ C_{23} & C_{33} & 0 \\ 0 & 0 & C_{44} \end{bmatrix} e^{(\alpha_1 y + \alpha_2 z)}$$
$$\mathbf{C}_{pn} = \mathbf{C}_{np}^T = \begin{bmatrix} C_{12} & 0 & 0 \\ C_{13} & 0 & 0 \\ 0 & 0 & 0 \end{bmatrix} e^{(\alpha_1 y + \alpha_2 z)} \tag{12}$$
$$\mathbf{C}_{nn} = \begin{bmatrix} C_{11} & 0 & 0 \\ 0 & C_{66} & 0 \\ 0 & 0 & C_{55} \end{bmatrix} e^{(\alpha_1 y + \alpha_2 z)}$$

Where the constant stiffness coefficients C_{ij} are:

$$C_{11} = C_{22} = C_{33} = \frac{1-\nu}{(1+\nu)(1-2\nu)} E_0 e^{(\beta_1+\beta_2)}$$
$$C_{12} = C_{13} = C_{23} = \frac{\nu}{(1+\nu)(1-2\nu)} E_0 e^{(\beta_1+\beta_2)} \tag{13}$$
$$C_{44} = C_{55} = C_{66} = \frac{1}{2(1+\nu)} E_0 e^{(\beta_1+\beta_2)}$$

3. HIERARCHICAL BEAM THEORIES

The variation of the displacement field towards y- and z-axis can be postulated a priori. Several displacement-based theories can be formulated on the basis of the following generic kinematic field:

$$\mathbf{u}(x, y, z) = F_\tau(y, z)\, \mathbf{u}_\tau(x) \quad \text{with} \quad \tau = 1, 2, \ldots, N_u \tag{14}$$

N_u stands for the number of unknowns. It depends on the approximation order N that is a free parameter of the formulation. The compact expression is based on Einstein's notation: subscript τ indicates summation. Thanks to this notation, problems governing differential equations and boundary conditions can be derived in a unified manner, that is, in terms of a single "fundamental nucleo." The complexity related to higher than classical approximation terms is tackled and the theoretical formulation is valid for the generic approximation order and approximating functions $F_\tau(y, z)$. In this paper, the functions F_τ are assumed to be the Mac Laurin's polynomials. This choice is inspired by the classical beam models. Table 1 presents N_u and F_τ as functions of N. They are obtained via Pascal's triangle. The actual governing differential equations and boundary conditions due to a fixed approximation order and polynomials' type are obtained straightforwardly via summation of the nucleo corresponding to each term of the expansion. According to the previous choice of polynomial function, the generic, N-order displacement field is:

$$\begin{aligned} u_x &= u_{x1} + u_{x2}y + u_{x3}z + \cdots + u_{x\frac{(N^2+N+2)}{2}} y^N \\ &\quad + \cdots + u_{x\frac{(N+1)(N+2)}{2}} z^N \\ u_y &= u_{y1} + u_{y2}y + u_{y3}z + \cdots + u_{y\frac{(N^2+N+2)}{2}} y^N \\ &\quad + \cdots + u_{y\frac{(N+1)(N+2)}{2}} z^N \\ u_z &= u_{z1} + u_{z2}y + u_{z3}z + \cdots + u_{z\frac{(N^2+N+2)}{2}} y^N \\ &\quad + \cdots + u_{z\frac{(N+1)(N+2)}{2}} z^N \end{aligned} \tag{15}$$

As far as the first-order approximation order is concerned, its kinematic field is obtained as particular case of Eq. (15):

$$\begin{aligned} u_x &= u_{x1} + u_{x2}y + u_{x3}z \\ u_y &= u_{y1} + u_{y2}y + u_{y3}z \\ u_z &= u_{z1} + u_{z2}y + u_{z3}z \end{aligned} \tag{16}$$

The classical beam models, such as TB:

$$\begin{aligned} u_x &= u_{x1} + u_{x2}y + u_{x3}z \\ u_y &= u_{y1} \\ u_z &= u_{z1} \end{aligned} \tag{17}$$

and EB:

$$\begin{aligned} u_x &= u_{x1} - u_{y1,x}y - u_{z1,x}z \\ u_y &= u_{y1} \\ u_z &= u_{z1} \end{aligned} \tag{18}$$

are straightforwardly derived from the first-order approximation model. In TB, no shear correction coefficient is considered, since it depends upon several parameters, such as the geometry of the cross-section (see Cowper [43] and Murty [44]).

Higher order models yield a more detailed description of the shear mechanics (no shear correction coefficient is required), the transverse to the section deformations, the coupling of the spatial directions due to Poisson's effect and the torsional mechanics than classical models do. EB theory neglects them all, since it was formulated to describe the bending mechanics. TB model accounts for constant shear stress and strain components. In the case of classical models and first-order approximation, the material stiffness coefficients should be corrected in order to contrast a phenomenon known in literature as Poisson's locking (see Carrera and Brischetto [45, 46]).

4. GOVERNING EQUATIONS

The strong form of the governing differential equations and the boundary conditions are obtained in terms of the displacement components and through the Principle of Virtual Displacements (PVD):

$$\delta L_i = \delta L_p + \delta L_l \tag{19}$$

L_i represents the strain energy. L_p and L_i stand for the work due to a surface loading, $\mathbf{p}^k$, and a line loading, l^k that act on a k sub-domain. δ stands for a virtual variation.

4.1. Variation of the Strain Energy

According to the grouping of the stress and strain components in Eqs. (4) and (5), the virtual variation of the strain energy is considered as sum of two contributes:

$$\delta L_i = \int_l \left(\int_{\Omega^k} \delta \epsilon_n^T \sigma_n \, d\Omega \right)_k dx + \int_l \left(\int_{\Omega^k} \delta \epsilon_p^T \sigma_p \, d\Omega \right)_k dx \tag{20}$$

By substitution of the geometrical relations, Eq. (7), the material constitutive equations, Eq. (10), and the unified hierarchical approximation of the displacements, Eq. (14), and after integration by parts, Eq. (20) reads:

$$\begin{aligned}
\delta L_i \int_l \delta \mathbf{u}_\tau^T \Bigg(\int_{\Omega^k} \big[& - \mathbf{D}_{nx}^T \mathbf{C}_{np}^k F_\tau (\mathbf{D}_p F_s \mathbf{I}) - \mathbf{D}_{nx}^T \mathbf{C}_{nn}^k F_\tau (\mathbf{D}_{np} F_s \mathbf{I}) \\
& - \mathbf{D}_{nx}^T \mathbf{C}_{nn}^k F_\tau F_s \mathbf{D}_{nx} + (\mathbf{D}_{np} F_\tau \mathbf{I})^T \mathbf{C}_{np}^k (\mathbf{D}_p F_s \mathbf{I}) \\
& + (\mathbf{D}_{np} F_\tau \mathbf{I})^T \mathbf{C}_{nn}^k (\mathbf{D}_{np} F_s \mathbf{I}) + (\mathbf{D}_{np} F_\tau \mathbf{I})^T \mathbf{C}_{nn}^k F_s \mathbf{D}_{nx} \\
& + (\mathbf{D}_p F_\tau \mathbf{I})^T \mathbf{C}_{pp}^k (\mathbf{D}_p F_s \mathbf{I}) + (\mathbf{D}_p F_\tau \mathbf{I})^T \mathbf{C}_{pn}^k (\mathbf{D}_{np} F_s \mathbf{I}) \\
& + (\mathbf{D}_p F_\tau \mathbf{I})^T \mathbf{C}_{pn}^k F_s \mathbf{D}_{nx} \big] d\Omega)_k \, \mathbf{u}_s \, dx \\
& + \Bigg[\delta \mathbf{u}_\tau^T \left(\int_{\Omega^k} F_\tau [\mathbf{C}_{np}^k (\mathbf{D}_p F_s \mathbf{I}) + \mathbf{C}_{nn}^k (\mathbf{D}_{np} F_s \mathbf{I}) \right. \\
& \left. + \mathbf{C}_{nn}^k F_s \mathbf{D}_{nx}] d\Omega \right)_k \mathbf{u}_s \Bigg]_{x=0}^{x=l}
\end{aligned} \tag{21}$$

The virtual variation of the strain energy in a compact vectorial form is:

$$\delta L_i = \int_l \delta \mathbf{u}_\tau^T \mathbf{K}^{\tau s} \, \mathbf{u}_s \, dx + \left[\delta \mathbf{u}_\tau^T \mathbf{\Pi}^{\tau s} \mathbf{u}_s \right]_{x=0}^{x=l} \tag{22}$$

The components of the differential matrix $\boldsymbol{K}^{\tau s}$ are:

$$\begin{aligned}
K_{xx}^{\tau s} &= \left(J_{\tau,_y s,_y}^{66k} + J_{\tau,_z s,_z}^{55k} - J_{\tau s}^{11k} \frac{\partial^2}{\partial x^2} \right)_k \\
K_{yy}^{\tau s} &= \left(J_{\tau,_y s,_y}^{22k} + J_{\tau,_z s,_z}^{44k} - J_{\tau s}^{66k} \frac{\partial^2}{\partial x^2} \right)_k \\
K_{zz}^{\tau s} &= \left(J_{\tau,_y s,_y}^{44k} + J_{\tau,_z s,_z}^{33k} - J_{\tau s}^{55k} \frac{\partial^2}{\partial x^2} \right)_k \\
K_{xy}^{\tau s} &= \left(-J_{\tau s,_y}^{12k} + J_{\tau,_y s}^{66k} \right)_k \frac{\partial}{\partial x} \quad K_{yx}^{\tau s} = \left(J_{\tau,_y s}^{12k} - J_{\tau s,_y}^{66k} \right)_k \frac{\partial}{\partial x} \\
K_{xz}^{\tau s} &= \left(-J_{\tau s,_z}^{13k} + J_{\tau,_z s}^{55k} \right)_k \frac{\partial}{\partial x} \quad K_{zx}^{\tau s} = \left(J_{\tau,_z s}^{13k} + J_{\tau s,_z}^{55k} \right)_k \frac{\partial}{\partial x} \\
K_{yz}^{\tau s} &= \left(J_{\tau,_y s,_z}^{23k} + J_{\tau,_z s,_y}^{44k} \right)_k \quad K_{zy}^{\tau s} = \left(J_{\tau,_z s,_y}^{23k} + J_{\tau,_y s,_z}^{44k} \right)_k
\end{aligned} \tag{23}$$

The generic terms $J_{\tau,_\phi s,_\xi}^{ggk}$, $J_{\tau s}^{ggk}$, $J_{\tau,_\phi s}^{ghk}$ and $J_{\tau s,_\phi}^{ghk}$ are the cross-section inertial momenta of a k sub-domain that account for the material gradation:

$$\begin{aligned}
J_{\tau,_\phi s,_\xi}^{ggk} &= \int_{\Omega^k} C_{gg}^k e^{(\alpha_1 y + \alpha_2 z)} F_{\tau,_\phi} F_{s,_\xi} \, d\Omega \\
J_{\tau s}^{ggk} &= \int_{\Omega^k} C_{gg}^k e^{(\alpha_1 y + \alpha_2 z)} F_\tau F_s \, d\Omega \\
J_{\tau,_\phi s}^{ghk} &= \int_{\Omega^k} C_{gh}^k e^{(\alpha_1 y + \alpha_2 z)} F_{\tau,_\phi} F_s \, d\Omega \\
J_{\tau s,_\phi}^{ghk} &= \int_{\Omega^k} C_{gh}^k e^{(\alpha_1 y + \alpha_2 z)} F_\tau F_{s,_\phi} \, d\Omega
\end{aligned} \tag{24}$$

Their analytical solution is presented in Appendix A. As far as the boundary conditions are concerned, the components of $\mathbf{\Pi}^{\tau s}$ are:

$$\begin{aligned}
\prod_{xx}^{\tau s} &= \left(J_{\tau s}^{11k} \right)_k \frac{\partial}{\partial x} \prod_{xy}^{\tau s} = \left(J_{\tau s,_y}^{12k} \right)_k \quad \prod_{xz}^{\tau s} = \left(J_{\tau s,_z}^{13k} \right)_k \\
\prod_{yy}^{\tau s} &= \left(J_{\tau s}^{66k} \right)_k \frac{\partial}{\partial x} \prod_{yx}^{\tau s} = \left(J_{\tau s,_y}^{66k} \right)_k \prod_{yz}^{\tau s} = 0 \\
\prod_{zz}^{\tau s} &= \left(J_{\tau s}^{55k} \right)_k \frac{\partial}{\partial x} \prod_{zx}^{\tau s} = \left(J_{\tau s,_z}^{55k} \right)_k \prod_{zy}^{\tau s} = 0
\end{aligned} \tag{25}$$

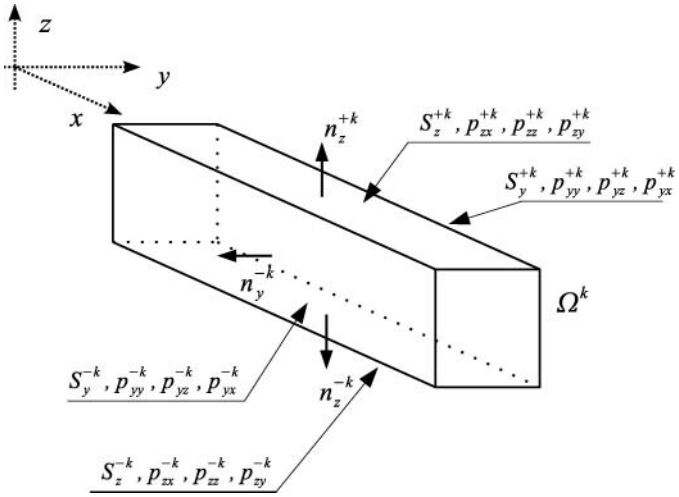

FIG. 3. Components of a surface loading, lateral surfaces and normal vectors of a k sub-domain.

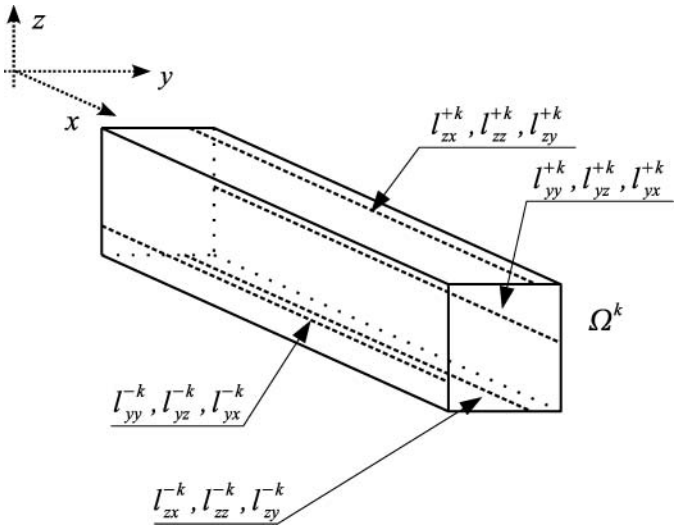

FIG. 4. Components of a line loading acting on a k sub-domain.

4.2. Virtual Work of the External Loadings

The virtual work done by the external loadings is assumed to be due to surface and line loadings.

4.2.1. *Surface Loading*

The components of a surface loading, p^k, that acts on a k sub-domain are:

$$\mathrm{p}^{kT} = \left\{ p_{zz}^{\pm k} \;\; p_{zx}^{\pm k} \;\; p_{zy}^{\pm k} \;\; p_{yy}^{\pm k} \;\; p_{yx}^{\pm k} \;\; p_{yz}^{\pm k} \right\} \tag{26}$$

They are applied as shown in Fig. 3. The lateral surfaces $\{S_\phi^{\pm k} : \phi = y, z\}$ of a k sub-domain are defined on the basis of the normal versor $\{n_\phi^{\pm k} : \phi = y, z\}$. A normal versor with the same orientation as y or z axis identifies a positive lateral surface. The total external virtual work is:

$$\delta L_p = \left(\delta L^k_{p^+_{zz}} + \delta L^k_{p^\pm_{zx}} + \delta L^k_{p^\pm_{zy}} + \delta L^k_{p^\pm_{yy}} + \delta L^k_{p^\pm_{yx}} + \delta L^k_{p^\pm_{yz}} \right)_k \tag{27}$$

Its explicit terms are:

$$\begin{aligned}
\left(\delta L^k_{p^\pm_{zx}}, \delta L^k_{p^\pm_{yx}} \right) &= \int_l \delta u_{x\tau} \left(p_{zx}^{\pm k} E_\tau^{kz^\pm}, p_{yx}^{\pm k} E_\tau^{ky^\pm} \right) dx \\
\left(\delta L^k_{p^\pm_{yy}}, \delta L^k_{p^\pm_{zy}} \right) &= \int_l \delta u_{y\tau} \left(p_{yy}^{\pm k} E_\tau^{ky^\pm}, p_{zy}^{\pm k} E_\tau^{kz^\pm} \right) dx \\
\left(\delta L^k_{p^\pm_{zz}}, \delta L^k_{p^\pm_{yz}} \right) &= \int_l \delta u_{z\tau} \left(p_{zz}^{\pm k} E_\tau^{kz^\pm}, p_{yz}^{\pm k} E_\tau^{ky^\pm} \right) dx
\end{aligned} \tag{28}$$

where:

$$\begin{aligned}
\left(E_\tau^{kz^+}, E_\tau^{kz^-} \right) &= \int_{y_1^k}^{y_2^k} \left(F_\tau(y, z_2^k), F_\tau(y, z_k^1) \right) dy \\
\left(E_\tau^{ky^+}, E_\tau^{ky^-} \right) &= \int_{z_1^k}^{z_2^k} \left(F_\tau(y_2^k, z), F_\tau(y_1^k, z) \right) dz
\end{aligned} \tag{29}$$

The closed form solution of the integrals in Eq. (29) is presented in Appendix A.

4.2.2. *Line Loading*

The components of a line loading (see Fig. 4) are:

$$\mathrm{l}^{kT} = \left\{ l_{zz}^{\pm k} \quad l_{zx}^{\pm k} \quad l_{zy}^{\pm k} \quad l_{yy}^{\pm k} \quad l_{yx}^{\pm k} \quad l_{yz}^{\pm k} \right\} \tag{30}$$

The external virtual work is:

$$\delta L_i = \left(\delta L^k_{l^\pm_{zz}} + \delta L^k_{l^\pm_{zx}} + \delta L^k_{l^\pm_{zy}} + \delta L^k_{l^\pm_{yy}} + \delta L^k_{l^\pm_{yx}} + \delta L^k_{l^\pm_{yz}} \right)_k \tag{31}$$

whose terms are:

$$\begin{aligned}
\left(\delta L^k_{l^\pm_{zx}}, \; \delta L^k_{l^\pm_{yx}} \right) &= \int_l \delta u_{x\tau} \left(l_{zx}^{\pm k} F_\tau \left(y^k_{l^\pm_{zx}}, z^k_{l^\pm_{zx}} \right), \right. \\
&\qquad \left. l_{yx}^{\pm k} F_\tau \left(y^k_{l^\pm_{yx}}, z^k_{l^\pm_{yx}} \right) \right) dx \\
\left(\delta L^k_{l^\pm_{yy}}, \; \delta L^k_{l^\pm_{zy}} \right) &= \int_l \delta u_{y\tau} \left(l_{yy}^{\pm k} F_\tau \left(y^k_{l^\pm_{yy}}, z^k_{l^\pm_{yy}} \right), \right. \\
&\qquad \left. l_{zy}^{\pm k} F_\tau \left(y^k_{l^\pm_{zy}}, z^k_{l^\pm_{zy}} \right) \right) dx \\
\left(\delta L^k_{l^\pm_{zz}}, \; \delta L^k_{l^\pm_{yz}} \right) &= \int_l \delta u_{z\tau} \left(l_{zz}^{\pm k} F_\tau \left(y^k_{l^\pm_{zz}}, z^k_{l^\pm_{zz}} \right), \right. \\
&\qquad \left. l_{yz}^{\pm k} F_\tau \left(y^k_{l^\pm_{yz}}, z^k_{l^\pm_{yz}} \right) \right) dx
\end{aligned} \tag{32}$$

where $\{(y^k_{l_{\phi\xi}}, z^k_{l_{\phi\xi}}) : \phi = y, z; \xi = x, y, z\}$ are the coordinates of the line loading application point on the cross-section of a k sub-domain.

4.3. The Fundamental Nucleo

The explicit form of the fundamental nucleo of the governing equations is:

$$
\begin{aligned}
&\delta u_{x\tau}: -J^{11}_{\tau s} u_{xs,xx} + \left(J^{55}_{\tau,_z s,_z} + J^{66}_{\tau,_y s,_y}\right) u_{xs} + \left(J^{66}_{\tau,_y s} - J^{12}_{\tau s,_y}\right) u_{ys,x} \\
&\quad + \left(J^{55}_{\tau,_z s} - J^{13}_{\tau s,_z}\right) u_{zs,_x} = \Big[p^{\pm k}_{zx} E^{kz^\pm}_{\tau} + p^{\pm k}_{yx} E^{ky^\pm}_{\tau} \\
&\quad + l^{\pm k}_{zx} F_\tau\left(y^k_{l^\pm_{zx}}, z^k_{l^\pm_{zx}}\right) + l^{\pm k}_{yx} F_\tau\left(y^k_{l^\pm_{yx}}, z^k_{l^\pm_{yx}}\right)\Big]_k \\
&\delta u_{y\tau}: \left(J^{12}_{\tau,_y s} - J^{66}_{\tau s,_y}\right) u_{xs,_x} - J^{66}_{\tau s} u_{ys,_{xx}} + \left(J^{22}_{\tau,_y s,_y} + J^{44}_{\tau,_z s,_z}\right) u_{ys} \\
&\quad + \left(J^{23}_{\tau,_y s,_z} + J^{44}_{\tau,_z s,_y}\right) u_{zs} = \Big[p^{\pm k}_{yy} E^{ky^\pm}_{\tau} + p^{\pm k}_{zy} E^{kz^\pm}_{\tau} \\
&\quad + l^{\pm k}_{yy} F_\tau\left(y^k_{l^\pm_{yy}}, z^k_{l^\pm_{yy}}\right) + l^{\pm k}_{zy} F_\tau\left(y^k_{l^\pm_{zy}}, z^k_{l^\pm_{zy}}\right)\Big]_k \\
&\delta u_{z\tau}: \left(J^{13}_{\tau,_z s} - J^{55}_{\tau s,_z}\right) u_{xs,_x} + \left(J^{23}_{\tau,_z s,_y} + J^{44}_{\tau,_y s,_z}\right) u_{ys} - J^{55}_{\tau s} u_{zs,_{xx}} \\
&\quad + \left(J^{33}_{\tau,_z s,_z} + J^{44}_{\tau,_y s,_y}\right) u_{zs} = \Big[p^{\pm k}_{zz} E^{kz^\pm}_{\tau} + p^{\pm k}_{yz} E^{ky^\pm}_{\tau} \\
&\quad + l^{\pm k}_{yy} F_\tau\left(y^k_{l^\pm_{yy}}, z^k_{l^\pm_{yy}}\right) + l^{\pm k}_{zy} F_\tau\left(y^k_{l^\pm_{zy}}, z^k_{l^\pm_{zy}}\right)\Big]_k
\end{aligned}
\tag{33}
$$

In the previous equations, the global cross-section momenta are adopted, that is, terms in Eq. (24) have been summed over all the sub-domains. The boundary conditions are:

$$
\begin{aligned}
&\left[\delta u_{x\tau}\left(J^{11}_{\tau s} u_{xs,_x} + J^{12}_{\tau s,_y} u_{ys} + J^{13}_{\tau s,_z} u_{zs}\right)\right]^{x=l}_{x=0} = 0 \\
&\left[\delta u_{y\tau}\left(J^{66}_{\tau s,_y} u_{xs} + J^{66}_{\tau s} u_{ys,_x}\right)\right]^{x=l}_{x=0} = 0 \\
&\left[\delta u_{z\tau}\left(J^{55}_{\tau s,_z} u_{xs} + J^{55}_{\tau s} u_{zs,_x}\right)\right]^{x=l}_{x=0} = 0
\end{aligned}
\tag{34}
$$

For a fixed approximation order, the nucleo has to be expanded versus the indexes τ and s in order to obtain the governing equations and the boundary conditions of the desired model.

5. CLOSED FORM ANALYTICAL SOLUTION

The differential equations are solved via a Navier type solution, that is, the following displacement field is adopted:

$$
\begin{aligned}
u_x &= U_{x\tau} F_\tau(y, z) \cos(\alpha x) \\
u_y &= U_{y\tau} F_\tau(y, z) \sin(\alpha x) \\
u_z &= U_{z\tau} F_\tau(y, z) \sin(\alpha x)
\end{aligned}
\tag{35}
$$

upon the assumption that the external loadings vary towards x in the following manner:

$$
\begin{aligned}
\mathbf{p}^{kT} &= \left\{P^{\pm k}_{zz} \sin(\alpha x)\, P^{\pm k}_{zx} \cos(\alpha x)\, P^{\pm k}_{zy} \sin(\alpha x)\, P^{\pm k}_{yy}\right. \\
&\quad \left. \times \sin(\alpha x)\, P^{\pm k}_{yx} \cos(\alpha x)\, P^{\pm k}_{yz} \sin(\alpha x)\right\} \\
\mathbf{l}^{kT} &= \left\{L^{\pm k}_{zz} \sin(\alpha x)\, L^{\pm k}_{zx} \cos(\alpha x)\, L^{\pm k}_{zy} \sin(\alpha x)\, L^{\pm k}_{yy}\right. \\
&\quad \left. \times \sin(\alpha x)\, L^{\pm k}_{yx} \cos(\alpha x)\, L^{\pm k}_{yz} \sin(\alpha x)\right\}
\end{aligned}
\tag{36}
$$

This assumption does not represent a loss in generality, since a generic loading can be approximated via its Fourier's series expansion (see Carrera and Giunta [47, 48]). Term α is:

$$
\alpha = \frac{m\pi}{l} \tag{37}
$$

where m represents the half-wave number along the beam axis. $\{U_{i\tau} : i = x, y, z\}$ are the maximal amplitudes of the displacement components and $\{P^{\pm k}_{i,j} : i = y, z; j = x, y, z\}$ and $\{L^{\pm k}_{i,j} : i = y, z; j = x, y, z\}$ the maximal amplitudes of the surface and line loading, respectively. The displacement field in Eq. (35) satisfies the boundary conditions since:

$$
\begin{aligned}
u_{x\tau,_x}(0) &= u_{x\tau,_x}(l) = 0 \\
u_{y\tau}(0) &= u_{y\tau}(l) = 0 \\
u_{z\tau}(0) &= u_{z\tau}(l) = 0
\end{aligned}
\tag{38}
$$

Upon substitution of Eqs. (35) and (36) into Eq. (33), the fundamental algebraic nucleo is obtained:

$$
\begin{aligned}
&\delta U_{x\tau}: \\
&\left(\alpha^2 J^{11}_{\tau s} + J^{55}_{\tau,_z s,_z} + J^{66}_{\tau,_y s,_y}\right) U_{xs} + \alpha\left(J^{66}_{\tau,_y s} - J^{12}_{\tau s,_y}\right) U_{ys} \\
&+\alpha\left(J^{55}_{\tau,_z s} - J^{13}_{\tau s,_z}\right) U_{zs} = \Big[P^{\pm k}_{zx} E^{kz^\pm}_{\tau} + P^{\pm k}_{yx} E^{ky^\pm}_{\tau} \\
&+L^{\pm k}_{zx} F_\tau\left(y^k_{l^\pm_{zx}}, z^k_{l^\pm_{zx}}\right) + L^{\pm k}_{yx} F_\tau\left(y^k_{l^\pm_{yx}}, z^k_{l^\pm_{yx}}\right)\Big]_k \\
&\delta U_{y\tau}: \\
&\alpha\left(J^{66}_{\tau s,_y} - J^{12}_{\tau,_y s}\right) U_{xs} + \left(\alpha^2 J^{66}_{\tau s} + J^{22}_{\tau,_y s,_y} + J^{44}_{\tau,_z s,_z}\right) U_{ys} \\
&+\left(J^{23}_{\tau,_y s,_z} + J^{44}_{\tau,_z s,_y}\right) U_{zs} = \Big[P^{\pm k}_{yy} E^{ky^\pm}_{\tau} + P^{\pm k}_{zy} E^{kz^\pm}_{\tau} \\
&+L^{\pm k}_{yy} F_\tau\left(y^k_{l^\pm_{yy}}, z^k_{l^\pm_{yy}}\right) + L^{\pm k}_{zy} F_\tau\left(y^k_{l^\pm_{zy}}, z^k_{l^\pm_{zy}}\right)\Big]_k \\
&\delta U_{z\tau}: \\
&\alpha\left(J^{55}_{\tau s,_z} - J^{13}_{\tau,_z s}\right) U_{xs} + \left(J^{23}_{\tau,_z s,_y} + J^{44}_{\tau,_y s,_z}\right) U_{ys} + \left(\alpha^2 J^{55}_{\tau s}\right. \\
&\left.+J^{33}_{\tau,_z s,_z} + J^{44}_{\tau,_y s,_y}\right) U_{zs} = \Big[P^{\pm k}_{zz} E^{kz^\pm}_{\tau} + P^{\pm k}_{yz} E^{ky^\pm}_{\tau} \\
&+L^{\pm k}_{yy} F_\tau\left(y^k_{l^\pm_{yy}}, z^k_{l^\pm_{yy}}\right) + L^{\pm k}_{zy} F_\tau\left(y^k_{l^\pm_{zy}}, z^k_{l^\pm_{zy}}\right)\Big]_k
\end{aligned}
\tag{39}
$$

For a fixed approximation order, the algebraic system has to be assembled according to the summation indexes τ and s. Its solution yields the maximal displacement amplitudes. The strains are retrieved by the geometric relations, Eq. (10), and the stresses via the generalised Hooke Law, Eq. (7).

6. NUMERICAL RESULTS AND DISCUSSION

Two numerical examples are presented to illustrate the accuracy of the proposed models. Results are compared with reference solutions that are present in literature or three-dimensional FEM models. Analyses account for slender and deep beams. Young's modulus is considered to vary exponentially with respect to z or both y and z coordinates. Poisson's ratio is constant. Beams are supposed to undergo bending and coupled bending-torsion loadings.

TABLE 2
Transverse displacement and stresses for $l/a = 100$, $\nu = 0.25$, loading acting on S_z^+

	$10^{-3}\bar{u}_z(\frac{l}{2}, 0)$	$10^{-2}\bar{\sigma}_{xx}(\frac{l}{2}, 0)$	$10^{-1}\bar{\sigma}_{xz}(0, \frac{a}{2})$	$10^{-1}\bar{\sigma}_{xz}(0, a)$	$\bar{\sigma}_{zz}(\frac{l}{2}, a)$	$\bar{\sigma}_{zz}(\frac{l}{2}, 0)$
N = 7	−4.0318	26.928	−4.4586	0.0000	−1.0000	0.0000
N = 6	−4.0318	26.928	−4.4583	−0.0008	−0.9986	0.0005
N = 5	−4.0318	26.928	−4.4607	−0.0076	−1.0108	0.0036
N = 3	−4.0318	26.928	−4.3508	−0.3718	−1.2152	0.0658
N = 1	−4.0318	26.928	−2.5752	−0.8143	−0.8397	−0.0840
TB	−4.0318	26.928	−2.5753	−0.8144	–	–
EB	−4.0311	26.927	–	–	–	–

6.1. Beam under Bending Loading

The beam undergoes a sinusoidal pressure of maximal amplitude P_{zz} and $m = 1$. It acts either on the top surface (S_z^+) or on the bottom one (S_z^-). The reference system is such that: $0 \leq x \leq \ell$, $-b/2 \leq y \leq b/2$ and $0 \leq z \leq a$. An aspect ratio, a/b, equal to 100 is adopted. Due to this value, the third dimension (y) is negligible. The span-to-height ratio, l/a, is as high as 100 (slender beams) and as low as 2 (deep beams). Young's modulus is such that $E_0 = 1000$ N/mm^2, $\beta_1 = \beta_2 = \phi$, $\alpha_l = \phi$ and $E(z = a)/E_0 = 10$. Unless differently stated, Poisson's ratio is equal to 0.25. Results are put into a non-dimensionalised form according to the following formulas:

$$\bar{u}_z = \frac{u_z}{a}$$
$$(\bar{\sigma}_{xx}, \bar{\sigma}_{xz}, \bar{\sigma}_{zz}) = \frac{1}{|P_{zz}|}(\sigma_{xx}, \sigma_{xz}, \sigma_{zz}) \tag{40}$$

The transverse displacement and normal stress component $\bar{\sigma}_{xx}$ are evaluated at $x = l/2$ and $z = 0$. The shear stress component is evaluated at $x = 0$ for $z = \alpha/2$. In order to verify the fulfilment of the stress boundary conditions, $\bar{\sigma}_{xz}$ is computed also at $z = 0$ and the transverse normal stress component $\bar{\sigma}_{zz}$ is computed at beam top and bottom surfaces for $x = l/2$. Table 2 presents the results for the case of a slender beam. The theories all yield the same values for transverse displacement and normal stress $\bar{\sigma}_{xx}$. A seventh-order approximation is required to satisfy the stress boundary conditions within the accuracy of five significant digits. Results for $l/a = 10$ and 5 are reported in Table 3. For $l/a = 10$, results are validated toward an elasticity solution by Lü et al. [49] computed via the method presented by Sankar [33]. A fourth-order approximation is required to match the reference transverse displacement. In the case of normal and shear stress components, N should equal 6 and 7, respectively. For the sake of brevity, the values of the transverse shear stress and the component $\bar{\sigma}_{xx}$ at $z = 0$ and a are not reported. Results are the same as the case of a slender beam. Parabolic approximation seems to yield poorer results than linear approximation does. It should be noticed that comparison is made only in one point of the cross-section. Variation of transverse displacement and normal stress above the cross-section for $l/a = 10$ is shown in Figs. 5 and 6; $\bar{\sigma}_{xz}$ and $\bar{\sigma}_{zz}$ versus z/a for $l/a = 10$ are reported in Figs. 7 and 8. Second-order approximation represents a transition between classical and first-order models in one side

TABLE 3
Transverse displacement and stresses for $l/a = 10$ and 5, $\nu = 0.25$, loading acting on S_z^+

	$l/a = 10$			$l/a = 5$		
	$10\bar{u}_z(\frac{l}{2}, 0)$	$\bar{\sigma}_{xx}(\frac{l}{2}, 0)$	$\bar{\sigma}_{xz}(0, \frac{a}{2})$	$10^2\bar{u}_x(\frac{l}{2}, 0)$	$10\,\bar{\sigma}_{xx}(\frac{l}{2}, 0)$	$\bar{\sigma}_{xz}(0, \frac{a}{2})$
Ref. [49]	−4.0942	26.922	−4.4527	–	–	–
N = 7	−4.0942	26.922	−4.4527	−2.6742	67.235	−2.2171
N = 6	−4.0942	26.922	−4.4523	−2.6742	67.237	−2.2169
N = 5	−4.0942	26.923	−4.4548	−2.6742	67.247	−2.2183
N = 4	−4.0942	26.928	−4.4867	−2.6741	67.299	−2.2350
N = 3	−4.0938	26.942	−4.3468	−2.6731	67.434	−2.1671
N = 2	−4.0854	26.761	−3.4008	−2.6507	65.627	−1.6935
N = 1	−4.0954	26.953	−2.5694	−2.6758	67.575	−1.2760
TB	−4.0959	26.928	−2.5753	−2.6815	67.319	−1.2876
EB	−4.0311	26.928	–	−2.5195	67.319	–

TABLE 4
Stresses for $l/a = 2.5$, $\nu = 0.30$, loading acting on S_z^-

	$\bar{\sigma}_{xx}(\frac{l}{2}, 0)$	$\bar{\sigma}_{xx}(\frac{l}{2}, a)$	$\bar{\sigma}_{xz,\max}$	$\bar{\sigma}_{xz}(0, 0)$	$\bar{\sigma}_{xz}(0, a)$	$\bar{\sigma}_{zz}(\frac{l}{2}, 0)$	$\bar{\sigma}_{zz}(\frac{l}{2}, a)$
Ref. [50]	−1.8175	8.4440	1.2805	–	–	–	–
N = 8	−1.8175	8.4440	1.2822	0.0000	0.0000	−1.0000	0.0000
N = 7	−1.8175	8.4441	1.2822	0.0001	−0.0002	−1.0001	0.0004
N = 6	−1.8178	8.4428	1.2823	0.0007	0.0018	−1.0009	−0.0027
N = 5	−1.8195	8.4508	1.2789	0.0052	−0.0125	−1.0045	0.0143
N = 4	−1.8249	8.4156	1.2877	0.0290	0.0678	−1.0141	−0.0490
N = 3	−1.8354	8.5441	1.3554	0.1209	−0.2558	−1.0261	0.1435
N = 2	−1.5591	8.5318	1.1083	0.3989	1.0975	−0.5941	1.0947
N = 1	−1.6067	8.7992	1.7638	0.2606	1.7638	−0.1742	−1.7419
TB	−1.6830	8.0363	2.0359	0.2036	2.0359	—	—
EB	−1.6830	8.0363	—	—	—	–	—

and higher-order theories in the other one. Fig. 9 presents $\bar{u}_z$ and $\bar{\sigma}_{xx}$ versus z/a for deep beams. Third-order approximation matches the eighth-order one. This last model satisfies the stress boundary conditions all within the fixed accuracy. Table 4 presents the stress field for the problem addressed in Lü et al. [50]. The loading is applied on S_z^-, the Poisson ratio equals 0.3 and the span-to-height ratio is 2.5. Normal and transverse normal stress components are computed at beam top and bottom for $x = l/2$. Eighth-order theory matches the reference solution. Shear stress is computed at $z = 0$ and a for $x = 0$. Its maximum value is also reported. For this stress component, the difference between the reference solution and the eighth-order model is about 0.1%. This last model also satisfies the stress boundary conditions.

6.2. Beam under Torsion-Bending Loading and Bi-Directional FGM

A beam with square cross-section subjected to a line loading is investigated. Cross-section sides measure 100 mm. The span-to-heigh ratio is equal to 100, 10 and 5. Loading configuration and reference system are shown in Fig. 10. Maximal loading amplitude is L_{zz} and m equals the unity. The material exhibits a gradation along y and z directions both: $E_0 = 1000$ N/mm^2, α_i such that $E(b,0)\,/E_0 = E\,(0,\,a)\,/E_0 = 3$ and $\beta_i = 0$ with $i = 1$ and 2 (see Fig. 2). Poisson's ratio equals 0.3. Displacement components are put into a non-dimensionalised form as follows:

$$(\bar{u}_x, \bar{u}_y, \bar{u}_z) = \frac{1}{a}(u_x, u_y, u_z) \tag{41}$$

The displacement along x is computed at (0, b, 0), while u_y and u_z are evaluated at $(l/2, 0, a)$. Stress components are normalised with respect to the ratio between the cross-section area and the loading resultant:

$$(\bar{\sigma}_{xx}, \bar{\sigma}_{xz}, \bar{\sigma}_{xy}, \bar{\sigma}_{yy}, \bar{\sigma}_{zz}) = \frac{\pi}{2}\frac{ab}{2lL_{zz}}(\sigma_{xx}, \sigma_{xz}, \sigma_{xy}, \sigma_{yy}, \sigma_{zz}) \tag{42}$$

The normal stress component $\bar{\sigma}_{xx}$ is evaluated at $(l/2, b, 0)$. Shear stresses $\bar{\sigma}_{xz}$ and $\bar{\sigma}_{xy}$ are computed at $(0, 0, a/2)$ and $(0, b/2, a)$, respectively. Components $\bar{\sigma}_{yy}$ and $\bar{\sigma}_{zz}$ are considered only in the case of span-to-height-ratio equal to 5 for which a stress localisation is present in correspondence of the loading application area at the mid-span. These stresses are evaluated at

TABLE 5
Dimensionless displacements and stresses for $l/a = 100$, bending-torsion loading.

	$10\bar{u}_x$	$10^2\bar{u}_y$	$10^{-1}\bar{u}_z$	$10^{-2}\bar{\sigma}_{xx}$	$\bar{\sigma}_{xz}$	$\bar{\sigma}_{xy}$
FEM 3D[a]	7.3079	1.3672	3.9472	−1.0818	1.4111	2.0509
N = 8	7.3084	1.3676	3.9474	−1.0820	1.3927	2.0622
N = 4	7.3084	1.3649	3.9473	−1.0820	1.4090	2.1202
N = 3	7.3085	1.1459	3.9470	−1.0819	1.0198	1.3917
N = 2	7.3079	1.1063	3.9469	−1.0818	0.9109	1.2499
N = 1	7.3076	1.2244	3.9469	−1.0818	0.8400	1.2075
TB	7.3117	−0.0007	3.9450	−1.0824	0.2613	−0.0003

Elements' length for FEM 3D[a] model: 80 × 2 × 2 mm.

TABLE 6
Dimensionless displacements for $l/a = 10$ and 5, bending-torsion loading

	$10^4\bar{u}_x$	$10^4\bar{u}_y$ $l/a = 10$	$10^3\bar{u}_z$	$10^5\bar{u}_x$		$10^5\bar{u}_y$ $l/a = 5$	$10^4\bar{u}_z$
FEM 3D[b]	7.3599	1.3640	4.2546	FEM 3D[d]	9.3817	3.3834	3.2344
FEM 3D[C]	7.3594	1.3629	4.2547	FEM 3D[c]	9.3806	3.3802	3.2336
N = 8	7.3600	1.3657	4.2546	N = 8	9.3801	3.3985	3.2345
N = 5	7.3597	1.3614	4.2542	N = 5	9.3805	3.3728	3.2326
N = 4	7.3587	1.3540	4.2524	N = 4	9.3690	3.3020	3.2164
N = 3	7.3739	1.1375	4.2212	N = 3	9.4415	2.7797	3.1385
N = 2	7.3143	1.1008	4.2075	N = 2	9.1578	2.7104	3.1153
N = 1	7.2819	1.2215	4.1997	N= 1	9.0061	3.0322	3.1031
TB	7.6381	−0.0631	4.0281	TB	10.314	−0.4880	2.6996

Elements' sides length: FEM 3D[6] 4 × 2 × 2 mm; FEM 3D[c] 4 × 4 × 4 mm and FEM 3D[d] 2 × 2 × 2 mm.

$(l/2, 4b/25, 0)$ and $(l/2, 0, 3a/25)$, respectively. The proposed models are compared with a three-dimensional FEM solution developed via MSC.Nastran commercial code. The eight-node brick element "HEXA8" is used. This element has only translational degrees of freedom, see MSC.Nastran User's Guide [51]. The boundary conditions are imposed noticing that u_y and u_z are null at the beam tips, while the axial displacement component is null in correspondence of the mid-span. The mesh depends upon the span-to-heigh ratio. For $l/a = 100$, the element's length is 80 × 2 × 2 mm along x, y and z. This solution is addressed as FEM 3D[a]. For $l/a = 5$, two element sizes are considered: 4 × 2 × 2 mm (FEM 3D[b]) and 4 × 4 × 4 mm (FEM 3D[c]). In the case of l/a equal to 5, the three dimensions of each element are equal to 2 (FEM 3D[d]), 4 (FEM 3D[c]) mm. Each element is considered as homogeneous by referring to the material properties at its centre point. Table 5 presents the dimensionless displacement and stress components for a slender beam. The mechanics is mainly governed by bending since the u_y and u_z differ by three orders of magnitude and normal and shear stresses by two ones. TB theory yields good results for displacements (u_x and u_z) and stress (α_{xx}) components that are due to bending. Transverse displacement component u_y and shear stress components are heavily underestimated.

The introduction of the linear terms for the displacements on the cross-section improves the solution. Increasing the expansion order, good convergence is shown. The proposed models match the reference FEM solution, the difference being about 1% in the case of α_{xz} computed via an eighth-order theory. Dimensionless displacements for $l/a = 10$ and 5 are reposted in Table 6. Fifth-order approximation matches the three-dimensional FEM solution. Fourth-order approximation yields good results, the difference being, at worse, about 2% for u_y and $l/a = 5$. Higher orders are required to describe the deformation due to the localised loading. Figs. 11 and 12 present the deformation of the cross-section at mid-span for $l/a = 10$ and 5, respectively. Tenth-order model yields very good results compared with solution FEM 3D[c]. Table 7 presents the dimensionless stresses for $l/a = 5$. For solution FEM 3D[c], shear stresses are computed as average between two consecutive nodes since the stresses are calculated at the element's centre and they are extrapolated out to the corner points only. The sudden change in slope in the neighbourhood of the loading application area is due to the presence of a high displacement gradient. A higher number of

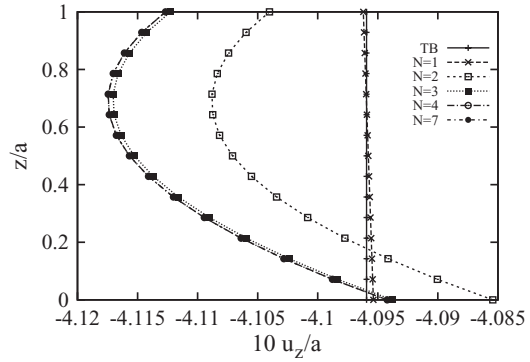

FIG. 5. Dimensionless transverse displacement at $x = l/2$ versus z/a for $l/a = 10$, beam under bending.

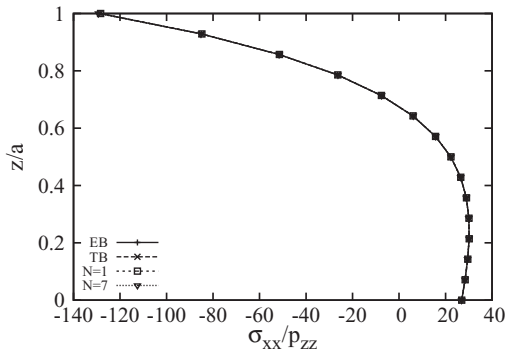

FIG. 6. Dimensionless normal stress at $x = l/2$ versus z/a for $l/a = 10$, beam under bending.

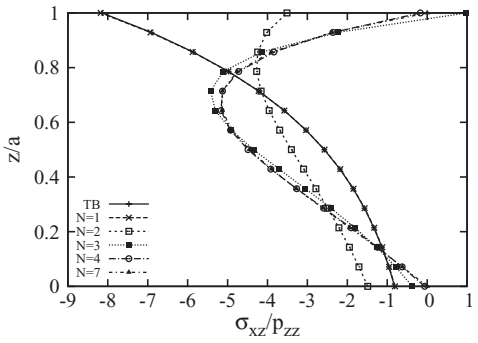

FIG. 7. Dimensionless transverse shear stress at $x = 0$ versus z/a for $l/a = 10$, beam under bending.

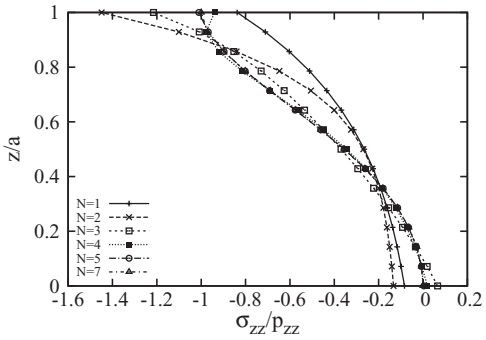

FIG. 8. Dimensionless transverse normal stress at $x = l/2$ versus z/a for $l/a = 10$, beam under bending.

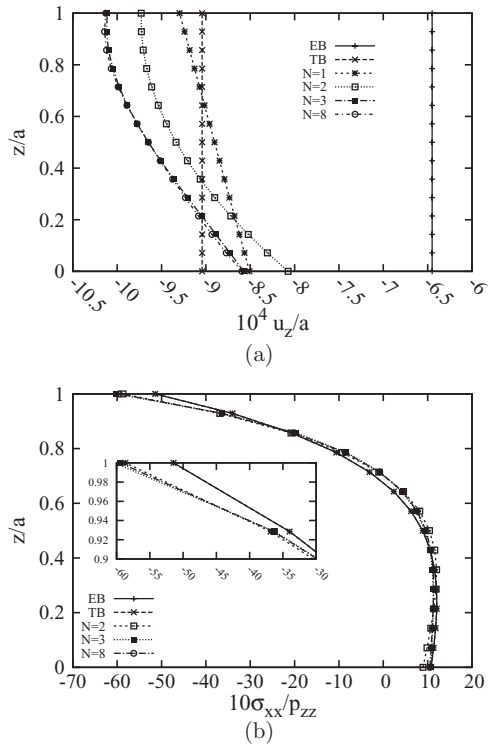

FIG. 9. Dimensionless transverse displacement and normal stress at $x = l/2$ versus z/a for $l/a = 2$, beam under bending.

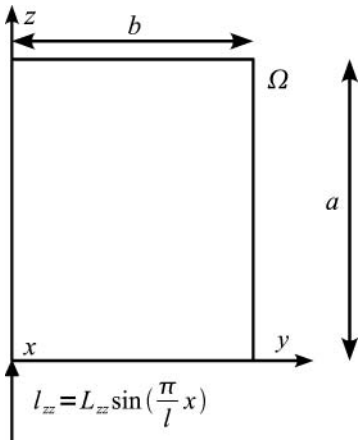

FIG. 10. Beam subjected to bending-torsion.

nodes is required in that area in order to obtain a variation that is smoother and closer to the actual behaviour. Good results are obtained for the normal and shear stress components, being the difference versus the three-dimensional solutions about 2% for $N = 8$, at worst. In the case of the transverse normal stress components, the difference is about 5%. This is due to the fact that such components are computed in the neighbourhood of the loading application area and the stress field is highly three-dimensional. The two reference FEM solutions differ there by about 2.5%. In this case a layer-wise approach is required. In such models, the displacement field is locally approximated, see Carrera [37]. This will matter in further development of the proposed approach to the one-dimensional modelling. As far as the computational costs are concerned, the proposed analytical models require less than a second, regardless of the approximation order. The FEM solution based on the proposed models, not reported here for the sake of brevity, is obtained in a few seconds for a very fine mesh. For the reference three-dimensional FEM solutions, FEM 3D^a, FEM 3D^b and FEM 3D^d require about two hours, while for FEM 3D^c results have been obtained after five and two minutes in the case of $l/a = 10$ and 5, respectively.

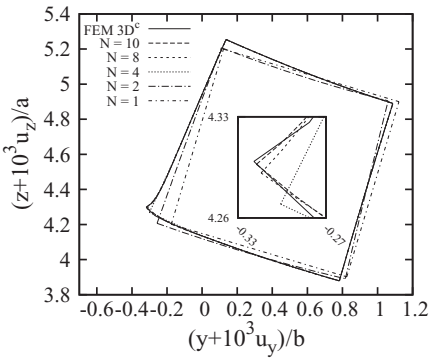

FIG. 11. Cross-section deformation at $x = l/2$ for $l/a = 10$, beam under bending-torsion loading.

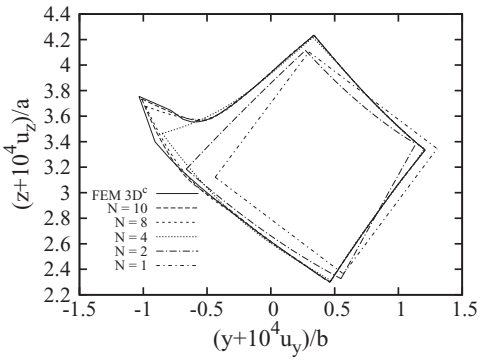

FIG. 12. Cross-section deformation at $x = l/2$ for $l/a = 5$, beam under bending-torsion loading.

TABLE 7
Dimensionless stresses for $l/a = 5$, bending-torsion loading.

	$\bar{\sigma}_{xx}$	$\bar{\sigma}_{yy}$	$\bar{\sigma}_{zz}$	$\bar{\sigma}_{xz}$	$\bar{\sigma}_{xy}$
FEM 3D^d	−5.5559	2.6328	−5.4280	1.4465	1.9920
FEM 3D^c	−5.5550	2.6675	−5.5675	1.4586*	1.9658*
N = 8	−5.6420	2.5120	−5.6689	1.4173	2.0032
N = 7	−5.5082	2.0114	−4.8488	1.4440	2.0243
N = 6	−5.5341	1.5355	−3.9423	1.4544	2.0409
N = 5	−5.7766	1.0784	−2.9782	1.4762	2.0797
N = 4	−5.6257	0.6734	−2.0170	1.4589	2.0510
N = 3	−5.3970	0.3021	−1.1304	1.0628	1.3239
N = 2	−5.3173	0.0961	−0.4096	0.9401	1.2334
N= 1	−5.3332	0.0164	−0.0660	0.8510	1.1875
TB	−6.1078	—	—	0.2568	−0.0939

Elements' sides length: FEM 3D^d 2 × 2 × 2 mm; FEM 3D^c 4 × 4 × 4 mm. (*) Average value of two consecutive nodes.

7. CONCLUSIONS

A unified formulation for modelling of beam structures made of functionally graded materials has been proposed. Higher order models that account for shear deformations and in- and out-of-plane warping can be formulated straightforwardly. It should be noted that the description of warping does not require any specific warping-function but it derives from the formulation itself. A classical models, such as Euler-Bernoulli's and Timoshenko's, are regarded as particular cases. A closed form, Navier type solution has been adopted. Beams subjected to bending and bending-torsional loadings have been investigated. Material gradation according to an exponential law function along one or two directions on the cross-section has been accounted for. The proposed formulation allows one to obtain results as accurate as desired through an appropriate choice of the approximation order. Classical models are accurate where the mechanics is governed by global bending, that is, for slender beams. The second-order model can be regarded as a transition between classical models and refined, higher order theories. Higher order models yield an accurate description of the three-dimensional mechanics as it has been show through comparison with reference solutions and three-dimensional FEM models. Higher order models are able to capture localised effects due to the loading condition. The efficiency of the models is very high since the computational costs are of the order of 10^{-1} seconds, while three-dimensional FEM models require several hours, in the case of a very fine mesh. The assumption of a polynomial law function for the material properties will be a matter of further investigation. In such a manner, a generic gradation law can be accounted for via its polynomial approximation.

ACKNOWLEDGMENTS

The first author is supported by the Ministère de la Culture, de 1'Enseignement Supérieuer et de la Recherche of Luxembourg under AFR-Postdoc grant TR-PDR BFR07-136.

REFERENCES

1. M. Koizumi, FGM Activities in Japan. Composites Part B: Engineering, vol. 28, no. 1–2, pp. 1–4, 1997.
2. J.N. Reddy, Analysis of Functionally Graded Plates, Int. J. Numer. Method Eng., vol. 47, no. 1–2, pp. 663–684, 2000.
3. J. Aboudi, M.J. Pindera, and S.M. Arnold, Higher-Order Theory for Functionally Graded Materials, Composites Part B: Engineering, vol. 30, no. 8, pp. 777–832, 1999.
4. Y.S. Shabana and N. Noda, Thermo-Elasto-Plastic Stresses in Functionally Graded Materials Subjected to Thermal Loading Taking Residual Stresses for the Fabrication Process into Consideration, Composites Part B: Engineering, vol. 32, no. 2, pp. 111–121, 2001.
5. F. Erdogan, Fracture Mechanics of Functionally Graded Materials, Composites Engineering, vol. 5, no. 7, pp. 753–770, 1995.
6. H.T. Xiao, Z.Q. Yue, L.G. Tham, et al., Stress Intensity Factors for Penny-Shaped Cracks Perpendicular to Graded Interfacial Zone of Bonded Bi-Materials, Eng. Fract. Mech., vol. 72, no. 1, pp. 121–143, 2005.
7. C.Y. Jian, T. Hashida, H. Takahashi, et al., Thermal Shock and Fatigue Resistance Evaluation of Functionally Graded Coating for Gas Turbine Blades by Laser Heating Method, Compos. Eng., vol. 5, no. 7, pp. 879–889, 1995.
8. W.Pompe, H. Worch, M. Epple, et al., Functionally Graded Materials for Biomedical Applications, Mater. Sci. Eng. A, vol. 362, no. 1–2, pp. 40–60, 2003.
9. E. Müller, C. Drasar, J. Schilz, et al., Functionally Graded Materials for Sensor and Energy Applications. Mater. Sci. Eng. A, vol. 362, no. l–2, pp. 17–39, 2003.
10. U. Schulz, M. Peters, F.W. Bach, et al., Graded Coatings for Thermal, Wear and Corrosion Barriers, Mater. Sci. Eng. A, vol. 362, no. 1–2, pp. 61–80, 2003.
11. S. Suresh and A. Mortensen, Fundamentals of Functional Graded Materials, IOM Communications Limited, London, UK, 1998.
12. Y. Miyamoto, W.A. Kaysser, B.H. Rabin, et al., Functionally Graded Materials: Design, Processing and Applications, Kluwer Academic, Boston, MA, 1999.
13. R. Watanabe, T. Nishida, and T Hirai, Present Status of Research on Design and Processing of Functionally Graded Materials, Met. Mater. Int., vol. 9, no. 6, pp. 513–519, 2003.
14. R. Hill, A Self-Consistent Mechanics of Composite Materials, J. Mechanics and Physics of Solids, vol. 13, no. 4, pp. 213–222, 1965.

15. T. Mori and K. Tanaka, Average Stress in Matrix and Average Elastic Energy of Materials with Misfitting Inclusions, Acta Metallurgica, vol. 21, no. 5, pp. 571–574, 1973.
16. J. Aboudi, Mechanics of Composite Materials: A Unified Micromechanical Approach, Elsevier, The Netherlands, 1991.
17. S. Nemat-Nasser and M. Hori, Micromechanics: Overall Properties of heterogeneous materials, North-Holland, New York, 1993.
18. J.R. Zuiker and G.J. Dvorak, The Effective Properties of Functionally Graded Composites. I Extension of The Mori-Tanaka Method to Linearly Varying Fields, Compos. Eng., vol. 4, no. 1, pp. 19–35, 1994.
19. H.T. Wakashima and H. Tsukamoto, Micromechanical Approach to the Thermomechanics of Ceramic-Metal Gradient Materials. In 1st Symp. Functionally Gradient Materials, The Functionally Gradient Materials Forum, Sendai, Japan, pp. 19–26, 1990.
20. M. J. Pindera, J. Aboudi, and S. M. Arnold, Limitations of the Uncoupled Rve-Based Micromechanical Approach in the Analysis of Functional Graded Composites, Mech. Mat., vol. 20, no. 1, pp. 77–94, 1995.
21. J. Aboudi, M.J. Pindera, and S.M. Arnold, Elastic Response of Metal Matrix Composites with Tailored Microstructures to Thermal Gradients, Int. J. Solids Struct., vol. 31, no. 10, pp. 1393–1428, 1994.
22. J. Aboudi, M.J. Pindera, and S.M. Arnold, Thermoelastic Theory for the Response of Materials Functionally Graded in two Directions, Int. J. Solids Struct., vol. 33, no. 7, pp. 931–966, 1996.
23. A. Chakraborty, S. Gopalakrishnan, and J.N. Reddy, A New Beam Finite Element for the Analysis of Functionally Graded Materials, Int. J. Mech. Sci., vol. 45, no. 3, pp. 519–539, 2003.
24. S.P. Timoshenko, On The Corrections for Shear of the Differential Equation for Transverse Vibrations of Prismatic Bars, Philos. Mag., vol. 41, pp. 744–746, 1921.
25. S.P. Timoshenko, On The Transverse Vibrations of Bars of Uniform Cross Section, Philos. Mag., vol. 43, pp. 125–131, 1922.
26. S.P. Timoshenko and J.N. Goodier, Theory of Elasticity. McGraw-Hill, 1970.
27. X.F. Li, A Unified Approach for Analyzing Static and Dynamic Behaviors of Functionally Graded Timoshenko and Euler-Bernoulli Beams, J. Sound Vib., vol. 318, no. 4–5, pp. 1210–1229, 2008.
28. R. Kadoli, K. Akhtara, and N. Ganesanb, Static Analysis of Functionally Graded Beams Using Higher order Shear Deformation Theory, Appl. Math. Model., vol. 32, no. 12, pp. 2509–2525, 2008.
29. S. Kapuria, M. Bhattacharyya, and A.N. Kumarb, Bending and Free Vibration Response of Layered Functionally Graded Beams: A Theoretical Model and its Experimental Validation, Compos. Struct., vol. 82, no. 3, pp. 390–402, 2008.
30. Y. Tomota, K. Kuroki, T. Mori, et al., Tensile Deformation of Two-Ductile-Phase Alloys: Flow Curves of $a - j$ fe-cr-ni alloys. Mat. Sci. Eng., vol. 24, no. 1, pp. 85–94, 1976.
31. B.O. Sallai, A. Tounsi, I. Mechab, et al., A Theoretical Analysis of Fiexional Bending of al/al_2O_3 s-FGM Thick Beams, Compu. Mat. Sci., vol. 44, no. 4, pp. 1344—1350, 2009.
32. Y.L. Chung and S.H. Chi, The Residual Stress of Functionally Graded Materials, J. Chinese Institute of Civil and Hydraulic Engineering, vol. 13, pp. 1–9, 2001.
33. B.V. Sankar, An elasticity Solution for Functionally Graded Beams, Compos. Sci. Technol., vol. 61, no. 5, pp. 689–696, 2001.
34. H. Zhu and B.V. Sankar, A Combined Fourier Series-Galerkin Method for the Analysis of Functionally Graded Beams. J. Appl. Mech., vol. 71, no. 3, pp. 421–424, 2004.
35. J.H. Ding, D.J. Huang, and W.Q. Chen, Elasticity Solutions for Plane Anisotropic Functionally Graded Beams, Int. J. Solid Struct., vol. 44, no. 1, pp. 176–196, 2007.
36. K. Silverman, Orthotropic Beams Under Polynomial Loads. Proceeding ASCE, Journal of the Engineering Mechanics Division, vol. 90, pp. 293–319, 1964.
37. E. Carrera, Theories and Finite Elements for Multilayered Plates and Shells: a Unified Compact Formulation with Numerical Assessment and Benchmarking, Arch. Comput. Method Eng., vol. 10, no. 3, pp. 215–296, 2003.
38. E. Carrera, S. Brischetto, and A. Robaldo, Variable Kinematic Model for the Analysis of Functionally Graded Material Plates, AIAA Journal, vol. 46, no. 1, pp. 194–203, 2008.
39. S. Brischetto and E. Carrera, Advanced Mixed Theories for Bending Analysis of Functionally Graded Plates, Computers and Structures, vol. 2008. in press.
40. E. Reissner, On a Certain, Mixed Variational Theory and a Proposed Application, Int. J. Numer. Method Eng., vol. 20, pp. 1366–1368, 1984.
41. S. Brischetto, R. Leetsch, E. Carrera, et al., Thermo-Mechanical Bending of Functionally Graded Plates, J. Therm. Stresses, vol. 31, no. 3, pp. 286–308, 2008.
42. F. Delale and F. Erdogan, Crack Problem for a Nonhomogeneous Plane, J. Appl. Mech., vol. 50, no. 3, pp. 609–614, 1983.
43. G.R. Cowper, The Shear Co-Efficient in Timoshenko Beam Theory. J. Appl. Mech., vol. 33, no. 10, pp. 335–340, 1966.
44. A. V. K. Murty, Analysis of Short Beams, AIAA Journal, vol. 8, no. 11, pp. 2098–2100, 1970.
45. E. Carrera and S. Brischetto, Analysis of Thickness Locking in Classical, Refined and Mixed Multilayered Plate Theories, Compos. Struct., vol. 82, no. 4, pp. 549–562, 2008.
46. E. Carrera and S. Brischetto, Analysis of Thickness Locking in Classical, Refined and Mixed Theories for Layered Shells, Compos. Struct., vol. 85, no. 1, pp. 83–90, 2008.
47. E. Carrera, G. Giunta, and S. Brischetto, Hierarchical Closed form Solutions for Plates Bent by Localized Transverse Loadings. Journal of Zhejiang University SCIENCE A, vol. 8, no. 7, pp. 1026 1037, 2007.
48. E. Carrera and G. Giunta, Hierarchical Models for Failure Analysis of Plates Bent by Distributed and Localized Transverse Loadings, J. Zhejiang University S.A, vol. 9, no. 5, pp. 600–613, 2008.
49. C.F. Lü, W.Q. Chen, R.Q. et al., Semi-Analytical Elasticity Solutions for Bi-Directional Functionally Graded Beams, Int. J. Solid Struct., vol. 45, no. l, pp. 258–275, 2008.
50. C.F. Lü, W.Q. Chen, and Z. Zheng, Two-Dimensional Thermoelasticity Solution for Functionally Graded Thick Beams, Science in China Series G: Physics, Mechanics and Astronomy, vol. 49, no.4, pp. 451–460, 2006.
51. MSC.Nastran, MSC.Nastran 2001, Getting Started with MSC.Nastran, User's Guide, 2002.

APPENDIX
ANALYTICAL INTEGRATION OVER THE CROSS-SECTION

The analytical solution of the term $J^{ghk}_{\tau,\phi,s,\xi}$ in Eq. (24) is presented for a generic cross-section's sub-domains. The function that has to be integrated is the product between $F_\tau = y^i z^j$ and $F_s = y^\eta z^\theta$ or their derivatives and an exponential function of y or z accounting for the material gradation:

$$J^{ghk}_{\tau,\phi s,\xi} = C^k_{gh} k_y k_z \int_{y_1^k}^{y_2^k} e^{(\alpha_1 y)} y^{n_y}\, dy \int_{z_1^k}^{z_2^k} e^{(\alpha_2 z)} z^{n_z}\, dz \qquad (43)$$

where C^k_{gh} is a constant term due to the material and k_y and k_z are constant terms coming from differentiation with respect to

y and z, respectively. The analytical solution is:

$$J^{ghk}_{\tau,\phi s,\xi} = C^k_{gh} k_y k_z \sum_{\lambda=0}^{n_y} (-1)^{n_y-\lambda} \frac{n_y! e^{(\alpha_1 y)} y^\lambda}{\lambda! \alpha_1^{n_y+1-\lambda}} \Bigg|_{y_1^k}^{y_2^k} \times \sum_{\zeta=0}^{n_z} (-1)^{n_z-\zeta} \frac{n_z! e^{(\alpha_2 z)} z^\zeta}{\zeta! \alpha_2^{n_z+1-\zeta}} \Bigg|_{z_1^k}^{z_2^k} \tag{44}$$

It can be demonstrated that when α_1 and α_2 tend to zero, the case of no material gradation can be obtained:

$$\lim_{\alpha_1,\alpha_2\to 0} J^{ghk}_{\tau,\phi s,\xi} = C^k_{gh} \frac{k_y}{n_y+1} \left[\left(y_2^k\right)^{n_y+1} - \left(y_1^k\right)^{n_y+1} \right] \times \frac{k_z}{n_z+1} \left[\left(z_2^k\right)^{n_z+1} - \left(z_1^k\right)^{n_z+1} \right] \tag{45}$$

The analytical solution of the integrals due to the surface loadings is:

$$\left(E^{ky^+}_\tau, E^{ky^-}_\tau\right) = \frac{\left((y_2^k)^i, (y_1^k)^i\right)}{j+1} \left[(z_2^k)^{j+1} - (z_1^k)^{j+1} \right] \tag{46}$$

$$\left(E^{kz+}_\tau, E^{kz-}_\tau\right) = \frac{\left((z_2^k)^j, (z_1^k)^j\right)}{i+1} \left[(y_2^k)^{i+1} - (y_1^k)^{i+1} \right] \tag{47}$$